THESIS FOR THE DEGREE OF LICENTIATE OF ENGINEERING

Extending Transient Plane Source-Based Measurements for the Accurate Determination of Thermal Transport Properties in Polymers

Zijin Zeng

Department of Chemistry and Chemical Engineering

CHALMERS UNIVERSITY OF TECHNOLOGY

Gothenburg, Sweden 2024

Extending Transient Plane Source-Based Measurements for the Accurate Determination of Thermal Transport Properties in Polymers

Zijin Zeng

Technical report no 2024:10

Department of Chemistry and Chemical Engineering

Chalmers University of Technology

SE-412 96 Gothenburg

Sweden

Telephone + 46 (0)31-772 1000

Cover:

[A graph depicting typical results of the Transient Plane Source Scanning measurement presented in the fashion of a jigsaw puzzle.]

[tryckeriets namn]

Gothenburg, Sweden 2024

This project has received funding from the European Union's Horizon 2020 research and innovation programme under the Marie Skłodowska-Curie grant agreement No 9558

Extending Transient Plane Source-Based Measurements for the Accurate Determination of Thermal Transport Properties in Polymers

Zijin Zeng

Department of Chemistry and Chemical Engineering

Chalmers University of Technology

ABSTRACT

The Transient Plane Source (TPS) method is widely used for measuring the thermal conductivity and thermal diffusivity of materials, including the apparent cross-plane thermal conductivity of films, which incorporates the influence of thermal contact resistance. However, to precisely determine the intrinsic cross-plane thermal conductivity of films, the measurement procedure should be refined to decouple thermal contact resistance. Additionally, the TPS method has been adapted into the Transient Plane Source Scanning (TPPS) method to directly measure the heat capacity. While effective for materials with a thermal conductivity exceeding 1 W/(mK), the TPPS method may underestimate the heat capacity of materials with a low conductivity, such as polymers.

This thesis addresses these issues in two parts:

First, it explores the application of TPS in determining the intrinsic thermal conductivity of film samples. Thermal contact resistance in the measurements was carefully analysed considering experimental conditions such as sample thickness, mounting force, and the use of thermal interface materials. Finally, an optimized TPS-based method was proposed, which considerably mitigates the thermal contact resistance and provides the precise determination of intrinsic cross-plane thermal conductivity in polymer films.

Second, this thesis utilizes a finite-element numerical model to investigate the TPPS method for heat capacity measurement. Unlike conventional numerical models that require preset material properties, several key material properties in our model were tuned using experimental data. This enables the model to accurately simulate the experimental process. Consequently, the model provides correct heat capacity determinations for samples across a spectrum of thermal conductivities.

Keywords: *Transient Plane Source method, finite element simulation, heat capacity, cross-plane thermal conductivity, polymer.*

NOMENCLATURE

ΔT	temperature increase of the TPS sensor
q	heat flux by conduction
λ	thermal conductivity
T	temperature
ρ	density
C_p	the specific heat capacity
α	thermal diffusivity
$\lambda_{\parallel}$	in-plane thermal conductivity
$\lambda_{\perp}$	cross-plane thermal conductivity
R	resistance of sensor
R_0	initial resistance of sensor
a	temperature coefficient of resistance
ΔT_s	temperature increase at sample surface facing the sensor
ΔT_i	additional temperature increase introduced by thermal resistance between the sensor and the samples
P	heating power from sensor
r	equivalent radius of sensor
τ	dimensionless time
D	dimensionless time function
t	time
t_c	time correction factor
λ_R	radial thermal conductivity
λ_A	axial thermal conductivity
α_R	radial thermal diffusivity
R_{tot}	total thermal resistance
h	thickness of film sample
$\lambda_{\perp,a}$	apparent cross-plane thermal conductivity of film
$\lambda_{\perp,i}$	intrinsic cross-plane thermal conductivity of film
A	area of sensor
t_s	settling time
d	thickness of bulk sample

Q	heat loss
f	heat loss equation
f_h	heat loss equation in holder measurement
f_s	heat loss equation in sample measurement
d	mass
T_h	temperature increase in holder measurement
T_s	temperature increase in sample measurement
P_h	heating power in holder measurement
P_s	heating power in sample measurement
δ	average rate of temperature increase
R_c	thermal contact resistance
Φ	power from the heat source
ε_Q	relative error in determining heat loss
Q_s	heat loss in the sample measurement
T_0	measurement temperature
M_W	weight average molecular weight

GHP	guarded hot plate
LFA	laser flash analysis
TPS	transient plane source
TDTR	time-domain thermoreflectance
FDTR	frequency-domain thermoreflectance
TWM	temperature wave method
DSC	differential scanning calorimetry
TPSS	transient plane scanning source
TIM	thermal interface material
HDPE	high-density polyethylene
PP	polypropylene
PMMA	poly(methyl methacrylate)

PUBLICATIONS

This thesis consists of an extended summary of the following appended papers:

Paper I **Extending the Transient Plane Source Scanning Method for Determining the Specific Heat Capacity of Low Thermal Conductivity Materials through a Numerical Study**

Zijin Zeng, Christian Müller, Besira Mihiretie

Under review

Paper II **Determination of intrinsic cross-plane thermal conductivity of films through the Transient Plane Source measurements**

Zijin Zeng, Christian Müller, Besira Mihiretie

Manuscript in preparation

The author has published the following papers which are not included in the thesis:

Paper III **A Thermal Excitation Based Partial Discharge Detection Method for Cable Accessory**

Zerui Li, Kai Zhou, Xiangdong Xu, Pengfei Meng, Yao Fu, Zijin Zeng

IEEE Transactions on Power Delivery, **2023**

https://ieeexplore.ieee.org/abstract/document/10065520

CONTRIBUTION REPORT

Paper I Main author. Carried out experiment, simulation, data process. Wrote most of the paper.

Paper II Main author. Carried out experiment, simulation, data process. Wrote most of the paper.

Paper III Assisted in developing simulation model.

TABLE OF CONTENT

Chapter 1

INTRODUCTION

1.1 Heat transfer and thermal properties

Heat transfer, the exchange of energy between materials driven by a temperature gradient, is a ubiquitous physical phenomenon encountered in both our daily routines and diverse industrial processes. A thorough understanding of heat transfer mechanisms allows us to utilize energy more intelligently and efficiently, leading to substantial energy conservation and paving the way for a more sustainable future.

The mechanisms of heat transfer can be categorized into conduction, convection, and radiation. Heat conduction is the process by which heat passes through the material itself, without any macroscopic movement of the heated body. Convection refers to the transfer of heat by the relative motion of a heated body, either liquid or gas. Radiation is the process by which heat is transferred directly between distant portions of the body by electromagnetic radiation.

In heat conduction, the extent of heat exchange through a material is proportional to the negative gradient in the temperature ($-\nabla T$), which is known as Fourier's law. The Fourier's law can be expressed as follows,

$$q = -\lambda \nabla T \tag{1.1}$$

where q denotes the local heat flux by conduction, the constant of proportionality λ is the thermal conductivity, a material property measured in watts per meter-kelvin $(\mathrm{W}/(\mathrm{mK}))$. λ can be expressed as the product of density (ρ), heat capacity (C_p) and thermal diffusivity (α), which describes the rate of temperature spread through a material and is measured in square metres per second (m^2/s),

$$\lambda = \alpha \rho C_p \tag{1.2}$$

Knowledge of the thermal properties (λ, C_p, and α) of substance holds significant value across various applications. For instance, this knowledge is instrumental in optimizing thermal management systems in electronics[1-3] and electric vehicles[4,5] to enhance performance and durability. Additionally, within the realm of construction, a profound understanding of the thermal properties of building materials helps design innovative architectural designs that decrease reliance on active thermal control technologies like heating, ventilation, and air conditioning, thus substantially decreasing energy use[6,7]. Furthermore, establishing connections between thermal properties and microstructure in thermoelectric materials offers valuable insights for developing enhanced materials, thereby boosting the areas of waste heat recovery and portable power sources[8-10].

1.2 Techniques for Measuring Thermal Properties

Techniques for measuring thermal conductivity and thermal diffusivity

For the measurement of thermal conductivity in bulk samples, several well-established and commercially available methods exist, such as the Guarded Hot Plate (GHP) method[11,12], the Laser Flash Analysis (LFA)[13], and the Transient Plane Source (TPS) method[14]. The GHP method is a conventional steady-state method based on one-dimensional Fourier's law, with advantages of simplicity and high accuracy. However, this method requires relatively larger samples and long measurement time. The LFA is a time-dependent method that uses a laser to provide a one-dimensional (1D) heat flow across the sample. It obtains the thermal diffusivity by measuring the time heat needed to pass through the sample and derives thermal conductivity using Eq. 1.2. The TPS method is a time-dependent method, with high versatility and high reliability. It correlates thermal properties with the measured temperature increase of the sensor. More information regarding TPS is available in Chapter 2.

However, when dealing with micrometer-thick film samples, the conventional methods for thermal conductivity face challenges due to the small thickness of samples. Recently, the TPS method has been extended to measure the apparent $\lambda_\perp$ and intrinsic $\lambda_\perp$ of film samples[14-18]. However, further investigation is required to improve the measurement procedure for a broader range of samples and achieve greater accuracy in the results.

Whereas there are several practical methods available for film samples, including the 3-ω method[19], the Time-domain Thermoreflectance (TDTR)[20,21], and Frequency-domain Thermoreflectance (FDTR)[22,23], the Temperature Wave method (TWM)[24,25]. The 3-ω method utilizes a metal sensor deposited on the smooth sample surface, which offers a frequency-dependent heating power to manipulate the penetration depth of heat. This method enables the measurement of in-plane thermal conductivity ($\lambda_{\parallel}$) and cross-plane thermal conductivity ($\lambda_{\perp}$) of film samples. Both TDTR and FDTR are based on optics, providing an evident advantage of no thermal contact resistance (R_c) between the sensing element and the sample. This advantage enables these methods to accurately determine the thermal conductivity of much thinner films. On the other hand, in cases where samples exhibit low light absorption and reflection, an extra layer of transducer is required to be deposited on the surface of sample. This additional step may increase both the duration and expense of the measurement procedure. The TWM, another frequency-domain method, measures the thermal diffusivity of film and calculates thermal conductivity by combining thermal diffusivity with volumetric heat capacity.

Techniques for measuring heat capacity

For the measurement of heat capacity, several conventional methods are available, including drop calorimetry[26,27], Differential Scanning Calorimetry (DSC)[28]. Drop calorimetry is in a method which involves dropping a heated sample with known temperature into a coolant, and measuring the change of the coolant temperature to determine the heat capacity of the sample. It is a rapid and straightforward technique yet requiring careful management of heat loss. DSC, one of the most widely used methods, enables measurements of heat capacity in a broad range of temperature. The results from DSC are precise even when dealing with very small sample quantities.

In contrast to DSC, the TPS provides heat capacity measurement of relatively larger samples[29,30]. This technique obtains the thermal conductivity and thermal diffusivity from a single measurement. Then the volumetric heat capacity of the sample can be indirectly determined via the ratio between the thermal conductivity and thermal diffusivity. However, this method is valid only when the sample is isotropic and homogenous.

The Transient Plane Scanning Source (TPSS) methods[29,31] is an extended application of the TPS setup and enables direct measurement of the heat capacity. This technique handles large and/or inhomogeneous samples, such as batteries, textiles, and building composites.

However, this method currently finds its application restricted to samples with thermal conductivities exceeding 1 W/(mK)[29], excluding most polymers.

1.3 Aims and scope

This thesis aims to expand TPS-based methodologies for precisely measuring thermal properties of polymers and other materials with low thermal conductivity, aiming to enrich the field of thermal characterization.

The research conducted within this thesis can be divided into two parts:

The first part involves the determination of intrinsic $\lambda_{\perp}$ in film samples using the TPS method. A comprehensive evaluation of the TPS method has been conducted to understand its abilities and limitations pertaining to the measurement of polymer films. Consequently, a refined experimental approach has been recommended to increase the robustness and accuracy of the measurements.

The second part is dedicated to determining the heat capacity of polymer using the TPSS method. A thorough investigation was performed to identify potential inaccuracies in TPSS measurements. Subsequently, a data analysis method assisted with finite-element modelling was proposed, facilitating the accurate determination of polymer heat capacity.

Chapter 2

THE TRANSIENT PLANE SOURCE METHOD

First introduced in 1991, the TPS method is now a reliable and widely spread technique for measuring thermal properties[32]. For isotopic bulk materials, the TPS method is able to determine both thermal conductivity and thermal diffusivity through a single measurement. The volumetric heat capacity of the material can be indirectly derived[14] via $\lambda = \alpha\rho C_p$. In cases of anisotropic materials, or the rod like isotropic materials, The TPS method enables the determination of thermal conductivity along a specific axis, provided the heat capacity of the material is already known[14]. Therefore, the TPS method has been extended to the Transient Plane Source Scanning (TPSS) method for the direct measurement of the heat capacity of materials[31].

Performing the TPS measurements is straightforward and effortless. In a standard TPS measurement, a TPS sensor is sandwiched between two samples with identical properties (Fig. 2.1a). The sensor is a thin nickel structure with shape of double spiral (Fig. 2.1b), embedded between two insulation layers such as polyimide (Kapton), polytetrafluoroethylene (Teflon), or mica. Throughout the measurement, the sensor severs two functions simultaneously: (1) it heats up the surrounding materials (the samples) via Joule heating, and (2) it records consequent temperature increase, $\Delta T(t)$, through the resistance change of the sensor[14]:

$$R(t) = R_0[1 + a \cdot \Delta T(t)] \tag{2.1}$$

where $R(t)$ is the resistance of the sensor in time, R_0 the initial resistance of the sensor, a the temperature coefficient of resistance of the sensor. A typical $\Delta T(t)$ resulted from a TPS measurement is shown in Fig. 2.2a. More details on data analysis are available in the subsequent sections.

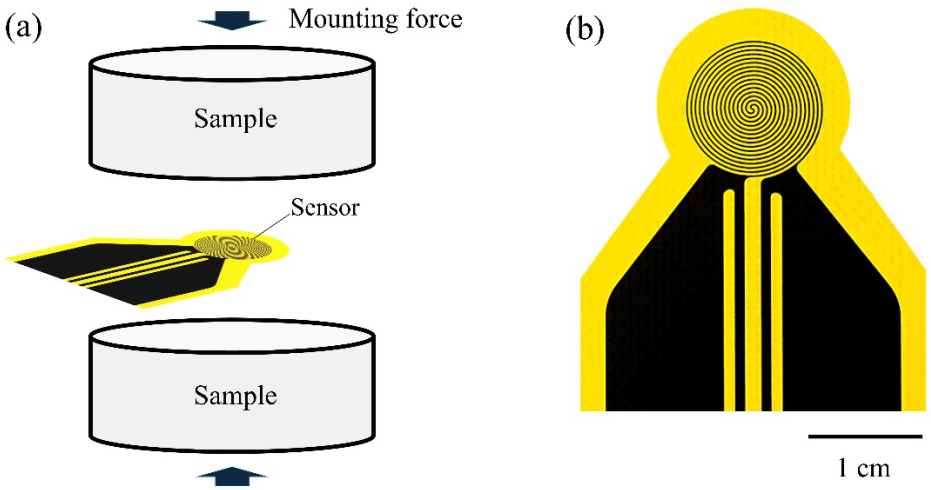

Figure 2.1. (a) Schematic sketch of a standard TPS measurement of bulk samples. (b) Profile of a TPS sensor encapsulated in insulation layers of polyimide.

2.1 Measurement of isotropic bulk samples

In the TPS measurement, $\Delta T(t)$ consists of two components, $\Delta T_s(t)$ and $\Delta T_i(t)$, as expressed as follow[14],

$$\Delta T(t) = \Delta T_i(t) + \Delta T_s(t) \tag{2.2}$$

where $\Delta T_s(t)$ denotes the temperature increase at the sample surface facing the sensor, while $\Delta T_i(t)$ is the additional temperature increase introduced by the thermal resistance between the sensor and the samples, which stabilizes to a constant value shortly after the measurement initiation.

In the TPS theory, it is assumed that the bifilar sensor can be approximated by a series of concentric and equally spaced circular line sources. This assumption gives a solution of heat transfer equation, which reveals the relationship between $\Delta T_s(\tau)$ and the thermal properties of isotropic samples[14].

$$\Delta T_s(\tau) = P\left(\pi^{3/2} r \lambda\right)^{-1} D(\tau) \tag{2.3}$$

where P is the heating power from the sensor, r is the equivalent radius of the sensor, and $D(\tau)$ represents a dimensionless time function of τ, which is defined as[14],

$$\tau = \left(\frac{t - t_c}{\theta}\right)^{1/2} \quad where \quad \theta = r^2/\alpha \tag{2.4}$$

where t_c denotes time correction factor for compensating unavoidable hardware and software delays.

Using the data of recorded $\Delta T(t)$, a least-squares iterative process is employed to optimize t_c and α. As suggested in Eq. 2.3, the iteration should result in a linear relationship between $D(\tau)$ and $\Delta T(t)$ (as shown in Fig. 2.2b). Afterwards, the thermal conductivity can be determined from the slope of the line.

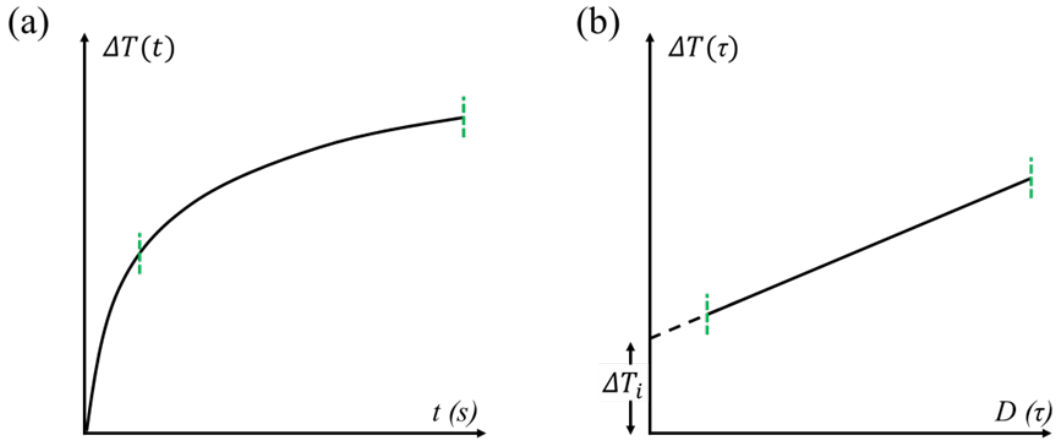

Figure 2.2. A typical temperature increase of sensor versus (a) time and (b) dimensionless time in the TPS measurement.

2.2 Measurement of anisotropic bulk samples

Utilizing the TPS method, it is also possible to measure both the thermal conductivity and the thermal diffusivity of anisotropic samples with uniaxial structure. Assuming that the properties of the samples are identical in the radial direction, with respect to the plane of the sensor, but different from that in the axial direction, the following equation can be used to describe $\Delta T_s(\tau)$ in the measurement[14],

$$\Delta T_s(\tau_R) = P\left(\pi^{3/2} r (\lambda_R \cdot \lambda_A)^{1/2}\right)^{-1} D(\tau_R) \tag{2.5}$$

where λ_R and λ_A are the radial and axial thermal conductivity, respectively[14].

$$\tau_R = \left(\frac{t - t_c}{\theta_R}\right)^{1/2} \quad where \quad \theta_R = r^2/\alpha_R \tag{2.6}$$

Similarly, an iteration using the data of $\Delta T(t)$ yields the radial thermal diffusivity, α_R. Then the radial thermal conductivity can be calculated with the equation $\lambda_R = \alpha_R \rho C_p$. Subsequently, λ_A can be calculated using Eq. 2.5[14].

2.3 Measurement of films cross-plane thermal conductivity

Theory

The TPS method can also be utilized to obtain the cross-plane thermal conductivity ($\lambda_{\perp}$) of film samples by employing a specially designed sensor with a broader nickel pattern (Fig. 2.3a)[14,17]. Measuring film samples requires two steps. The initial step requires performing a reference measurement with the sensor sandwiched between two pieces of bulk materials with relatively high thermal conductivity (referred to as background material from here on), as shown as Fig. 2.3b. The subsequent step is to perform a sample measurement with two films of identical properties positioned between the sensor and the background materials, respectively. It is crucial to apply the same mounting force in both measurements to ensure consistency.

As discussed before, $\Delta T_i(t)$ is related to the total thermal resistance between the sensor and the materials (R_{tot}). When utilizing a specially designed sensor (Fig. 2.3a) and assuming one-dimension heat flow across the sample, the correlation between the $\Delta T_i(t)$ and the R_{tot} could be described by[14],

$$P = 2A\Delta T_i / R_{tot} \tag{2.7}$$

where A is the area of the sensor. In reference measurement (Fig. 2.3b), the total thermal resistance, $R_{tot,r}$, consists of thermal contact resistance between the sensor and the background material ($R_{c,s-b}$) and the thermal resistance of the polyimide insulation layer (R_i). In sample measurement (Fig. 2.3c), the total thermal resistance $R_{tot,s}$ consists of R_i, thermal resistance of the film sample (R_f), the thermal contact resistance between the film sample and background material ($R_{c,f-b}$), as well as the thermal contact resistance between the sensor and the film ($R_{c,s-f}$). If $R_{c,s-b}$ approximate $R_{c,s-f}$ closely, the following equation can be used to calculate the apparent cross-plane thermal conductivity of the film samples ($\lambda_{\perp,a}$), which includes the influence of $R_{c,f-b}$,

$$\lambda_{\perp,a} = \Delta h(R_{tot,s} - R_{tot,r})^{-1} \tag{2.8}$$

where h represents the thickness of the film samples. If additional sample measurements of film samples with different thickness are implemented[15,16,18] (Fig. 2.3d), we can apply Eq. 2.9 to determine the intrinsic cross-plane thermal conductivity of the film ($\lambda_{f,i}$),

$$\lambda_{\perp,i} = \Delta h(\Delta R_{tot,s})^{-1} \tag{2.9}$$

However, the derivation of Eq. 2.9 is based on a fundamental assumption that $R_{c,f-b}$ and $R_{c,s-f}$ is independent to the sample thickness; in other words, $R_{c,f-b}$ and $R_{c,s-f}$ remains unchanged in these sample measurements.

If multiple sample pairs are measured, Eq. 2.9 can be extended to Eq. 2.10 to linearly fit the experimental data,

$$R_{tot,s} = R + h(\lambda_{\perp,i})^{-1} \tag{2.10}$$

The reciprocal of fit gives the value of $\lambda_{\perp,i}$, while the intercept R reflects the total thermal contact resistance in the measurement.

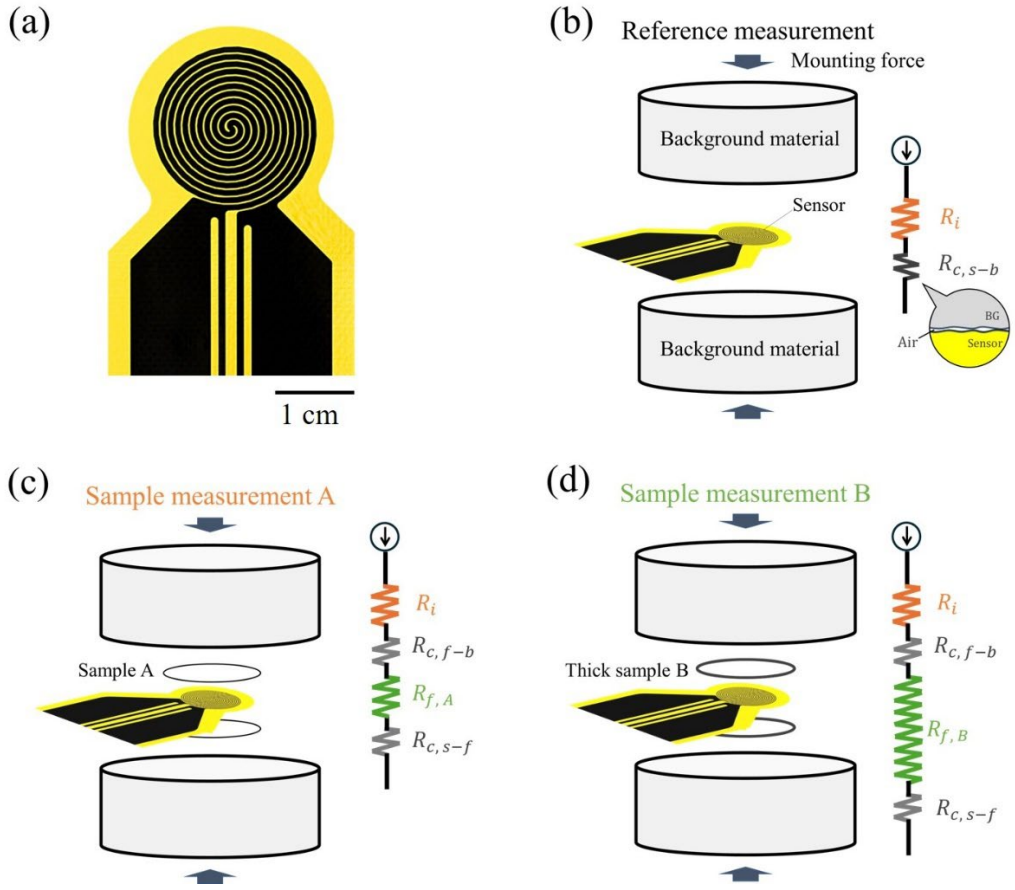

Figure 2.3. (a) Profile of a TPS sensor for film measurement, with the feature of wide bifilar spiral. (b-d) Schematic sketch of a (b) reference measurements, (c, d) sample measurements of films with different thickness, and their respective thermal networks.

Capabilities and limitations

The TPS method is capable of measuring the apparent cross-plane thermal conductivity of films with thickness ranging from 20 μm to 600 μm and thermal conductivity between 0.05 W/(mK) to 2 W/(mK), with an expected reproducibility of +/- 3%. While the theory and procedure of using the TPS method for measuring intrinsic thermal conductivity of film require further refinement which we discuss in **Chapter 3**.

2.4 Direct measurement of heat capacity (the TPSS measurement)

Theory

As mentioned before, the necessity of determining direction-dependent thermal properties motivates the development of the TPSS method, which aims to measure heat capacity directly. The TPSS method is an adaptation of the standard TPS, utilizing the same type of sensor but attached onto a specially designed sample holder (Fig. 2.4a).

Two steps are involved in the TPSS measurement as well. First, a measurement is performed with an empty sample holder, which we referred to as the holder measurement. The purpose of this initial step is to collect essential information regarding the heat capacity of the holder and the heat loss during the measurement. This is followed by a measurement incorporating a specimen within the sample holder (Fig. 2.4b), intended to collect the data containing the information about the heat capacity of the sample. During both measurements, the sample holder should be surrounded by thermal insulation materials to mitigate heat dissipation.

In TPPS measurements, there are two fundamental assumptions. The first is that the $\Delta T(t)$ recorded by the sensor can represent the average temperature increase of the sample after a settling time, t_s. The settling time can be approximated using the formula $t_s = 2d^2/\alpha$, where d is the thickness of the sample[29]. The second assumption is that there exists a heat loss equation, $f_h(t)$, which governs the rate of heat loss by $Q(t) = \frac{d}{dt}\big(\Delta T(t)\big)f(t)$. Based on these assumptions, Eq. 2.10 and Eq. 2.11 can be written for holder measurement and sample measurement, respectively[31],

$$P_h = [(mC_p)_h + f_h(t)]\frac{d}{dt}\big(\Delta T_h(t)\big) \tag{2.10}$$

$$P_s = [(mC_p)_h + (mC_p)_s + f_s(t)]\frac{d}{dt}\left(\Delta T_s(t)\right) \quad (2.11)$$

where $\frac{d}{dt}\left(\Delta T_s(t)\right)$ denotes the rate of temperature increase, subscript h and s represent holder measurement and sample measurement, respectively. For the sample measurement, the heating power from the sensor, P_s, should be carefully selected so that $\Delta T_s(t)$ is close to $\Delta T_h(t)$. In the phase of measurement where that $\Delta T_s(t)$ and $\Delta T_h(t)$ exhibit linear alignment[31], it is assumed that $f_h(t)$ is identical to $f_s(t)$. Combining Eq. (a) and Eq. (b), we can derive an equation to calculate the heat capacity of sample[31]:

$$\frac{\overline{P_s}}{\delta_s} - \frac{\overline{P_h}}{\delta_h} = \left(mC_p\right)_s \quad (2.12)$$

where $\overline{P}$ is the average heating power from the sensor and δ is the average rate of temperature increase, defined as $\frac{d}{dt}\overline{\Delta T_s(t)}$.

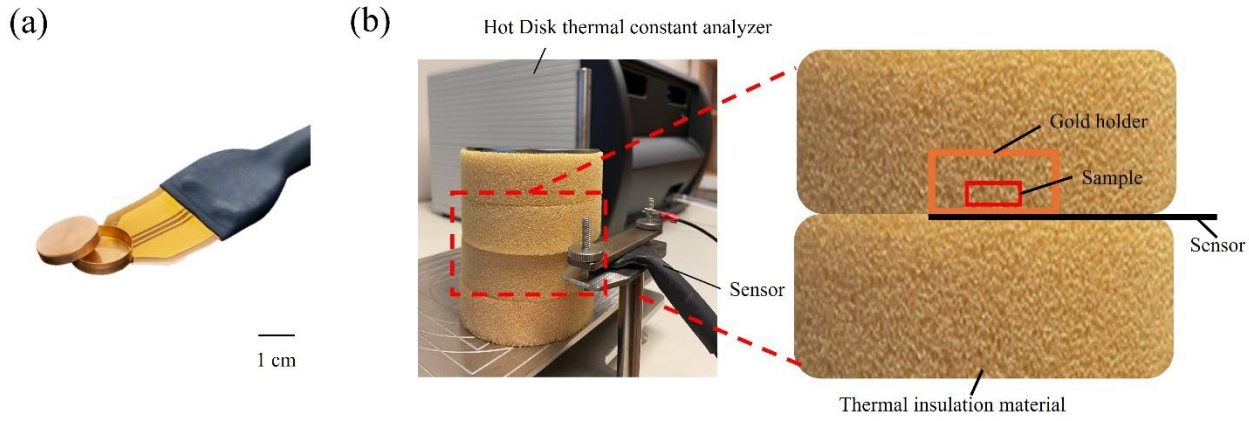

Figure 2.4. (a) A Hot Disk sensor attached to a gold sample holder. (b) Schematic diagram of a TPSS measurement with a sample.

Capabilities and limitations

TPPS is capable of determining the heat capacity of sample with thermal conductivity higher than 1 W/(mK), with a high reproducibility of +/- 2%. However, it tends to underestimate the materials with a low thermal conductivity (<1 W/(mK)) owing to the heat loss during the measurement process[33]. More details regarding the heat loss underestimation are available on **Paper II, Fig. 2b.**

Chapter 3

EXTENDING THE TPS METHOD FOR MEASURING INTRINSIC CORSS-PLANE THERMAL CONDUCTIVITY

In this chapter, we developed and validated a procedure for measuring intrinsic cross-plane thermal conductivity of films using the TPS method. We have taken into account the impact of crucial factors on measurement outcomes, such as sample flatness, mounting force, and the utilization of thermal interface materials (TIMs).

3.1 Sample preparation

We fabricated two types of film samples using high-density polyethylene (HDPE) and polypropylene (PP), respectively. The HDPE, obtained from Sigma-Aldrich (547999), has a weight average molecular weight (M_W) of 95 kg/mol and a polydispersity index of 5.3. The PP, obtained from Sigma-Aldrich (427888), has a M_W of 250 kg/mol and a polydispersity index of 3.7.

These materials were pressed into film shapes under a pressing force of 15 KN, using a laboratory press (LabPro 200) supplied by Fontijne Presses. The pressing temperature for HDPE and PP were 180°C and 210 °C, respectively. Utilizing a Constant Thickness Film Maker from Specac Ltd., we kept the film diameter at 29 mm while adjusting the thickness across twelve distinct levels within a range of 20 μm to 410 μm.

Nevertheless, the films generated through hot pressing exhibit deviations from perfect flatness. To quantify their flatness, we measured the film thickness at five distinct locations using a micrometer (Fig. 3.1, inset). The deviation of the measured values is calculated for each level of thickness (Fig. 3.1) to serve as a measure of the flatness of the films. The average deviation for all the film samples made by hot pressing is around 2 μm.

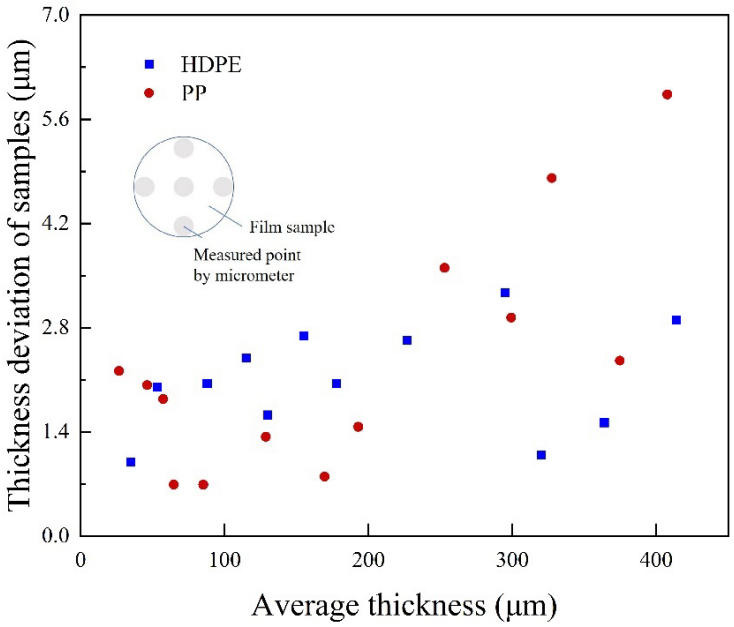

Figure 3.1. The thickness deviation of the film samples.

3.2 Measurement results

Through the TPS measurements, the total thermal resistance between the sensor and background material was determined. These obtained values were plotted against the thickness of the samples (Fig. 3.2). Subsequently, a linear fit based on Eq. 2.10 was applied to each set of results, resulting in respective slopes and intercepts. The reciprocal of the slope is expected to represent the intrinsic cross-plane thermal conductivity, while the intercepts are expected to yield information about the thermal contact resistance.

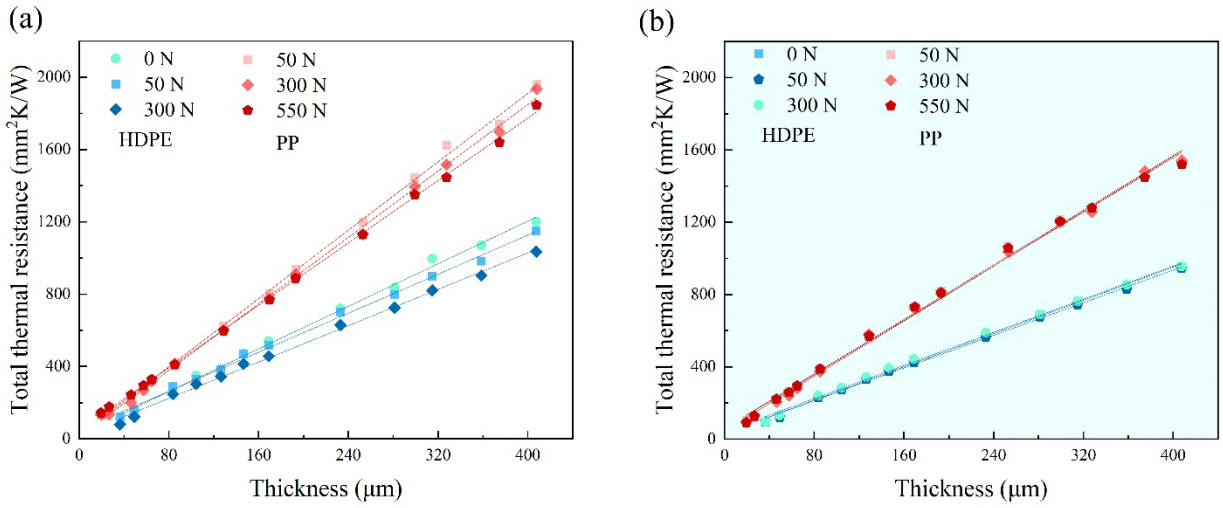

Figure 3.2. The total thermal resistance versus the thickness of the films in measurements at different mounting pressure: (a) without and (b) with deionized water as thermal interface material.

We investigated the influence of mounting force on the results of the total thermal resistance (Fig. 3.2a). Interestingly, we observed a notable decrease in total thermal resistance for thick samples compared to thin samples when applying higher mounting forces. Given that thin samples are more flexible than those thicker, we reasonably infer that thicker samples exhibit higher thermal contact resistance and thus have more potential for reduction. This deduction is contrary to the assumption made in Chapter 2.3.

The varying degree of reduction in total thermal resistance leads to a lower slope of the fit (Fig. 3.2a) and thus a higher calculated $\lambda_\perp$ (Table 3.1). Since the calculated $\lambda_\perp$ here is dependent on the mounting pressure, it is concluded that it is not the intrinsic $\lambda_\perp$ that we anticipated.

We repeated the measurements with the introduction of deionized water as liquid thermal material between the sensor, samples, and background materials. Remarkably, in this case, the values of total thermal resistance appear to be independent of mounting pressure. This can be attributed to the replacement of air trapped in the contact interfaces by water, which considerably reduces and stabilizes thermal contact resistance.

Finally, we calculated $\lambda_\perp$ from these measurements (Table 3.1), which exhibits a better alignment with reference value. Despite the significant difference in mounting force employed, the relative deviation of the extracted $\lambda_\perp$ is under 1%.

Table 3.1. The results from the fits in Fig. 3.2, including the intrinsic $\lambda_{\perp}$ (the reciprocal of the slope) and the intercept.

Material	Mounting force (N)	Calculated $\lambda_{\perp}$ (without TIM)	Intercept (without TIM)	Calculated $\lambda_{\perp}$ (with deionized water as TIM)	Intercept (with deionized water as TIM)
HDPE	0	0.340 ± 0.006	26.367 ± 11.747	0.436 ± 0.008	41.078 ± 9.031
	50	0.371 ± 0.007	47.158 ± 11.106	0.435 ± 0.006	31.657 ± 7.465
	300	0.398 ± 0.008	23.167 ± 10.982	0.443 ± 0.006	32.015 ± 7.190
PP	50	0.212 ± 0.002	4.724 ± 0.0480	0.265 ± 0.005	58.812 ± 15.646
	300	0.218 ± 0.003	12.326 ± 11.687	0.263 ± 0.004	44.756 ± 13.681
	550	0.232 ± 0.002	48.253 ± 7.178	0.267 ± 0.005	57.379 ± 15.369

3.3 Numerical simulation for potential error

In this section, we developed and employed numerical models to investigate potential errors in our measurements.

In the TPS method for film samples, it is assumed that the heat flow across the sample is 1D (Eq. 2.7). However, the heat flow in the actual scenario is more intricate, primarily due to two reasons. The first reason is that the actual pattern of the sensor is a wide double spiral, instead of an ideal circle as assumed in Eq. 2.7. Another reason is that film samples often have a slightly larger radius than the sensor for easier installation of the measurement. The inconsistency between the actual scenario and the idealized theory could introduce errors. Furthermore, the introduction of liquid thermal interface material may also contribute to errors. In this context, the numerical model is designed to estimate the error arising from these aforementioned factors.

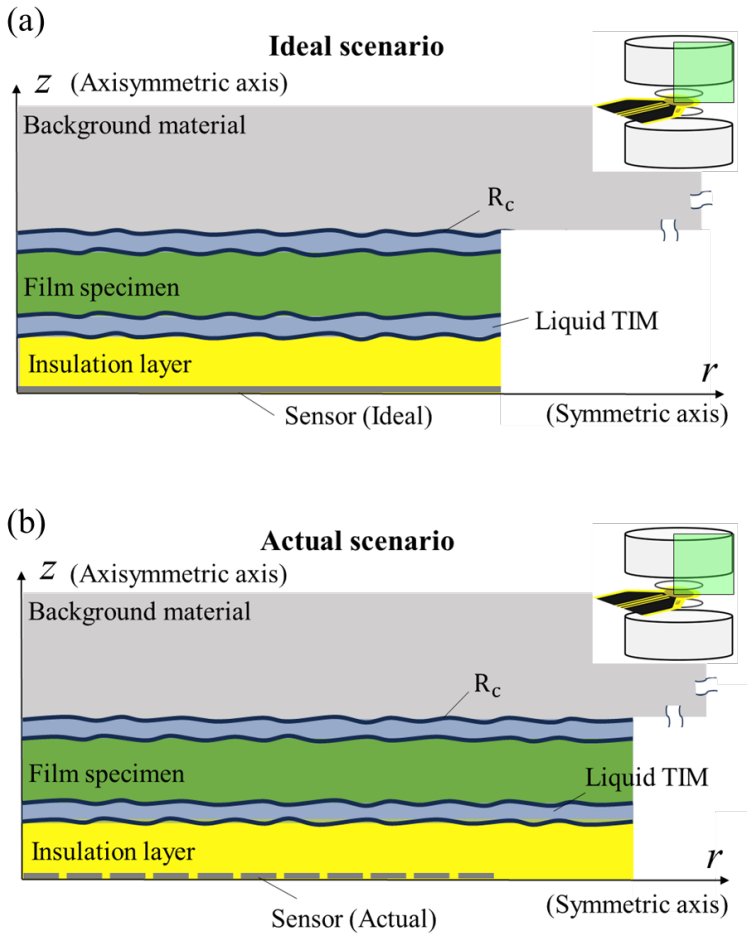

Figure 3.3 Schematic diagram of the numerical models of ideal 1D scenario (a) and the actual scenario (b).

These simulation models are developed in two-dimensional (2D) based on the following assumptions:

- The measurement components, including the sensor, background material, layers, and interfaces can be treated as asymmetric.
- The bifilar sensor pattern can be approximated as a sequence of concentric and uniformly spaced circular line sources.
- Heat transfer between measurement components and ambient environment is negligible (adiabatic boundary condition).
- Heat transfer via convection and radiation is negligible.
- Material properties are assumed to remain constant during the measurement.

The first numerical model is developed to mimic the scenario with 1D heat flow. Another model is constructed for the actual scenario with a more complex heat flow. The schematic diagrams of these two models are shown in Fig. 3.3a and b, respectively. Note that the thickness of the water layer was set to the average deviation of the sample thickness, 2 μm. Besides, the material properties used in the simulation are summarized in Table 3.2.

The simulation model is based on equations for non-steady state heat conduction, as presented below,

$$\rho C_p \frac{\partial T}{\partial t} + \nabla q = Q \tag{3.1}$$

$$q = -\lambda \nabla T \tag{3.2}$$

where q denotes heat flux by conduction, while Q is the power supplied from the heat source.

Table 3.2. Material properties used in the numerical simulation.

Component	Material	$\lambda\ (W/(mK))$	$C_p\ (J/kg/K)$	$\rho\ (kg/m^3)$
Background material	Stainless steel	13.7	460	8150
Insulation layer	Polyimide	0.18	1090	1420
Sensor pattern	Nickel	91.4	444	8900
Liquid TIM	Deionized water	0.6	4186	997

After the calculation, we obtained the simulated temperature distribution of the components (Fig. 3.4a). In the ideal scenario, the temperature evenly decreases from the sensor to the background material, suggesting 1D heat flow. On the other hand, in the actual scenario, temperature distribution deviates from the 1D assumption due to the geometry of the sensor pattern and the additional edge area. Subsequently, the difference in temperature increase between these two scenarios is obtained (Fig. 3.4b). This difference is dependent on both the thickness and thermal conductivity of the samples and ranges from -10% to 6%.

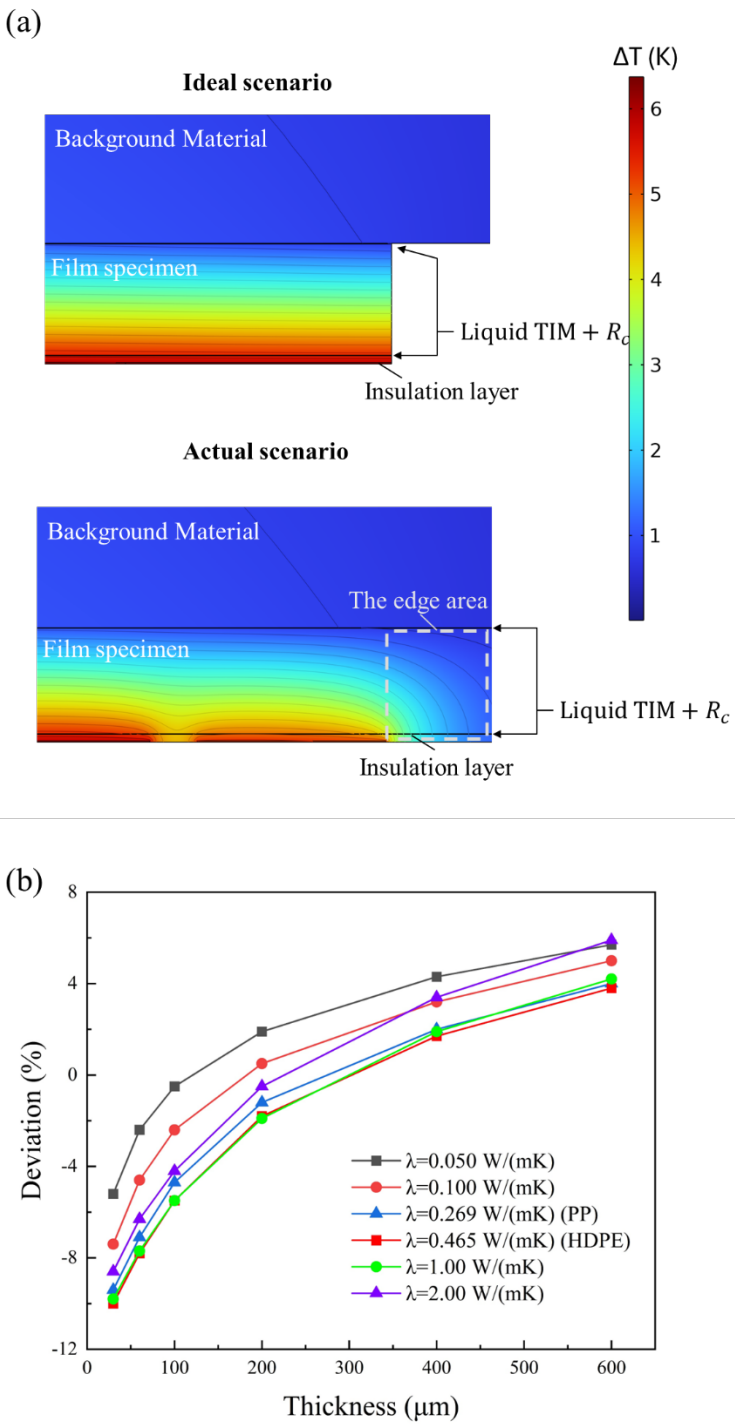

Fig. 3.4 (a) The comparison of temperature distribution across the film specimen between the ideal scenario and the actual scenario. (b) The relative deviation between the ideal scenario and the actual scenario.

3.4 Discussion and conclusion

With knowledge of the difference between the ideal and actual scenario, we calibrated the results in Fig. 3.2b. Furthermore, to evaluate the reproducibility and robustness of the current method, we recalculated the intrinsic $\lambda_{\perp}$ using smaller subsets of data points drawn from the calibrated dataset rather than the full array. Specifically, we implemented a loop to iteratively select pairs of sample points and recalculated the intrinsic $\lambda_{\perp}$. Then the results of recalculated intrinsic $\lambda_{\perp}$ were plotted against the thickness difference of the corresponding sample pairs (Fig. 3.5a). The analysis aims to demonstrate the feasibility of extracting a reliable intrinsic $\lambda_{\perp}$ with just two pair of samples.

As illustrated in Fig. 3.5a, the recalculated $\lambda_{\perp}$ displays more scatter when the thickness difference is small, possibly due to the higher uncertainty in measuring thin samples. Whereas the recalculated $\lambda_{\perp}$ converges as the thickness difference increases.

To refine our analysis, we excluded the data of the samples with thickness lower than 80 μm due to their relatively high uncertainty. Subsequently, a similar plot revealing the relationship between the intrinsic $\lambda_{\perp}$ and the thickness difference is generated (Fig. 3.5b). In this case, the data points are more concentrated, especially in the low thickness difference range. When the thickness difference exceeds 200 μm, the calculated $\lambda_{\perp}$ for HDPE and PP converges to 0.431 W/(mK) and 0.263 W/(mK), respectively, with a fluctuation being around 5%. This indicates that two pairs of samples could be adequate for a reliable measurement of $\lambda_{\perp}$, provided the thickness difference between them exceeds 200 μm.

Using the same routine, the intrinsic $\lambda_{\perp}$ of poly(3-hexylthiophene) (P3HT) films made by hot pressing was determined to be 0.198 W/(mK). More information about the P3HT can be found in **Paper I, Table IV**.

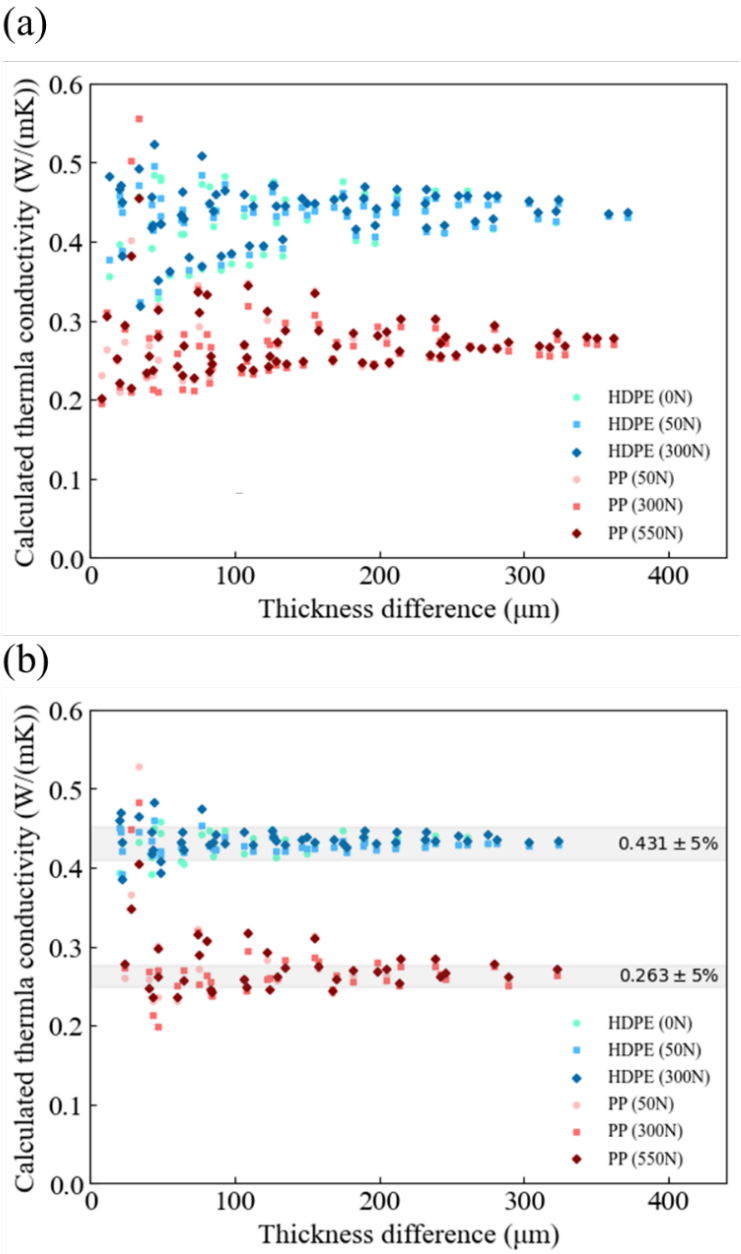

Fig. 3.5 (a) Calculated thermal conductivity versus thickness difference between the sample pairs. (b) Same as (a) but utilizing the data of samples with thickness larger than 80 μm.

Ultimately, we compared the extracted results from Fig. 3.5b and the reference values from the Temperature Wave method (TWM) and the TPS measurement of bulk samples (Table 3.3). The average difference between the extracted $\lambda_{\perp}$ and TWM value is 4.2% for HDPE and 8.7% for PP, respectively. The average difference between the extracted $\lambda_{\perp}$ and the values from the TPS measurements of bulk samples is 7.3 % and 2.2 % in the cases of HDPE and PP, respectively. Note that the difference between the reference values in the cases of HDPE and

PP is 3.2% and 10.0% respectively. These comparison results demonstrate the reliability of the proposed method in this work.

Table. 3.3. The comparison between the $\lambda_{\perp}$ from this work and the reference value from the Temperature wave method ($\lambda_{\perp,TWM}$) and the TPS measurement of bulk materials ($\lambda_{\perp,TPS}$). The $\lambda_{bulk,TPS}$ were obtained from the bulk specimens made by the same routine of hot pressing as the film specimens.

Material	$\lambda_{\perp}$ (W/(mK))	$\lambda_{\perp,TWM}$ (W/(mK))	$\lambda_{bulk,TPS}$(W/(mK))
HDPE	0.431 ± 0.022	0.450 ± 0.021	0.465 ± 0.001
PP	0.263 ± 0.013	0.242 ± 0.017	0.269 ± 0.001

In conclusion, this chapter presents a novel procedure for applying TPS-based measurements to extract the intrinsic $\lambda_{\perp}$ of film samples, even when faced with the challenge of uneven sample surfaces. We introduced deionized water as a thermal interface material in the measurements, which effectively reduces the thermal contact resistance and thus the uncertainty. Furthermore, numerical simulation was employed to estimate the extent of errors in the measurement caused by the discrepancy between theoretical assumptions and actual experimental conditions. The measurement data were then calibrated based on the knowledge of the errors and used for a refined evaluation of the results. Finally, this evaluation confirms that the proposed procedure can accurately determine the thermal conductivity of films, Finally, this evaluation confirms that the proposed procedure can accurately determine the thermal conductivity of film samples, as long as multiple paired samples are measured and the minimum thickness of the samples exceeds 80 μm.

Chapter 4

EXTENDING THE TPSS METHOD FOR MEASURING HEAT CAPACITY OF LOW THERMAL CONDUCTIVITY SAMPLES

In this chapter, numerical simulation is employed to study the cause of underestimated results for low thermal conductivity samples. A well-tuned model is developed to mimic the measurement process, thereby enabling the accurate estimation of the heat capacity of samples.

4.1 The development of a numerical model

To simplify the simulation model, we made the following the assumptions:

- The heat transfer between measurement setup and ambient environment is negligible (adiabatic boundary condition).
- Heat transfer via convection and radiation within the setup is negligible.
- The measurement setup is axisymmetric, rendering the effects from sensor leads and the non-circular shape of the sample negligible.
- Material properties remain constant during the measurement.
- The spiral sensing element of the sensor can be represented by an ideal circle boundary heat source.

Subsequently, the two-dimensional (2D) geometry of the model was constructed according to its experimental TPSS counterpart. The employment of 2D geometry aims at reducing computational overhead while maintaining accuracy in capturing the heat conduction during measurements. A detailed visualization of each component within the model is achieved through a 3D representation, created by rotating the 2D geometry (Fig. 4.1).

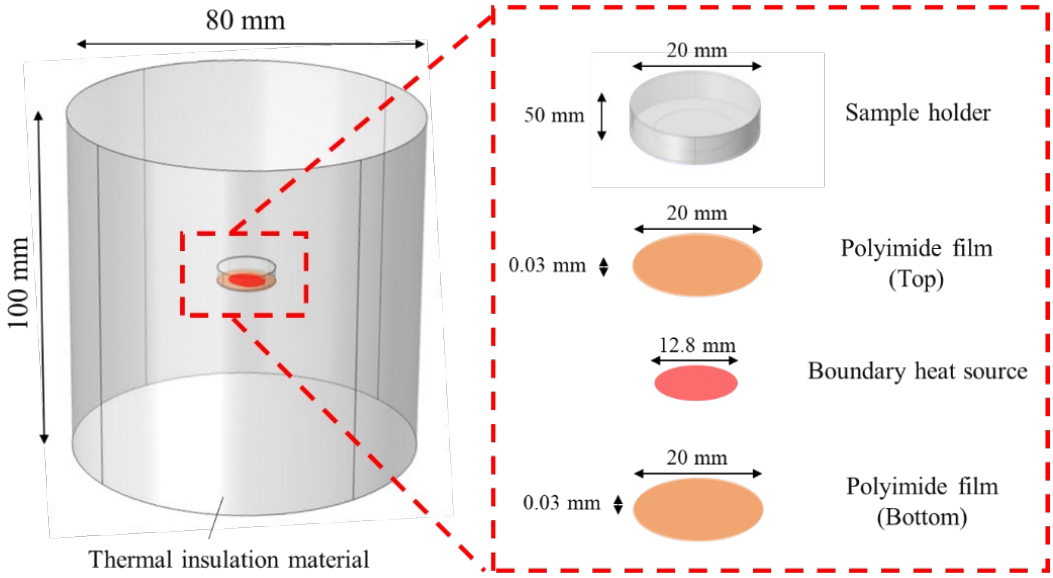

Figure 4.1. Schematic diagram of the model, which represents the simulation counterpart for the experimental setup depicted in Fig. 2.4b.

The material properties used in this numerical model are detailed in Table 4.1. The governing equation of the model is Eq. 3.1 and Eq. 3.2. A mesh independence study has been conducted to select the proper mesh configuration for the simulation.

Table 4.1. Summary of the component properties used in the numerical model. a. Measured by the TPS measurement for slab samples[14]. b. Calculated based on the specific heat capacity of the ingredients. c. Calculated from mass and volume. d. Measured by the TPS measurement for bulk samples[14]. e. Obtained from reference[34].

Component	Material	$\lambda\ (W/(mK))$	$C_p\ (J/kg/K)$	$\rho\ (kg/m^3)$
Sample holder	Gold alloy	44 ± 10^a	177^b	1065^c
Insulation Material	Polyimide foam	0.039 ± 0.04^d	1090^e	6.6^c
Polyimide film	Polyimide film	0.12^e	1090^e	1420^e

4.2 The development and utilization of the well-tuned model

The following outline illustrates the four steps for developing and utilizing the well-tuned model (Fig. 4.2).

The first step involves the development of a numerical model, as detailed in the previous section. Afterward, the numerical model is employed to conduct a sensitivity analysis, identifying the key material properties which dominate $\Delta T(t)$ in the measurement. The sensitivity analysis is detailed in **Paper II, Section 3.2**. The third step entails tuning these key material properties through a parameter estimation study within the numerical model, utilizing the $\Delta T(t)$ data from the holder measurement. Finally, sample geometry is incorporated into the model, while retaining the key material properties identified in the previous step. Another parameter estimation study is then conducted to estimate the heat capacity of the sample, utilizing the $\Delta T(t)$ data from the sample measurement.

The parameter estimation study is based on a derivative-free solver, bound optimization by quadratic approximation (BOBYQA), integrated within the commercial simulation software COMSOL Multiphysics. The core principle of the BOBYQA method involves iteratively approximating the objective function with a suitable quadratic model.

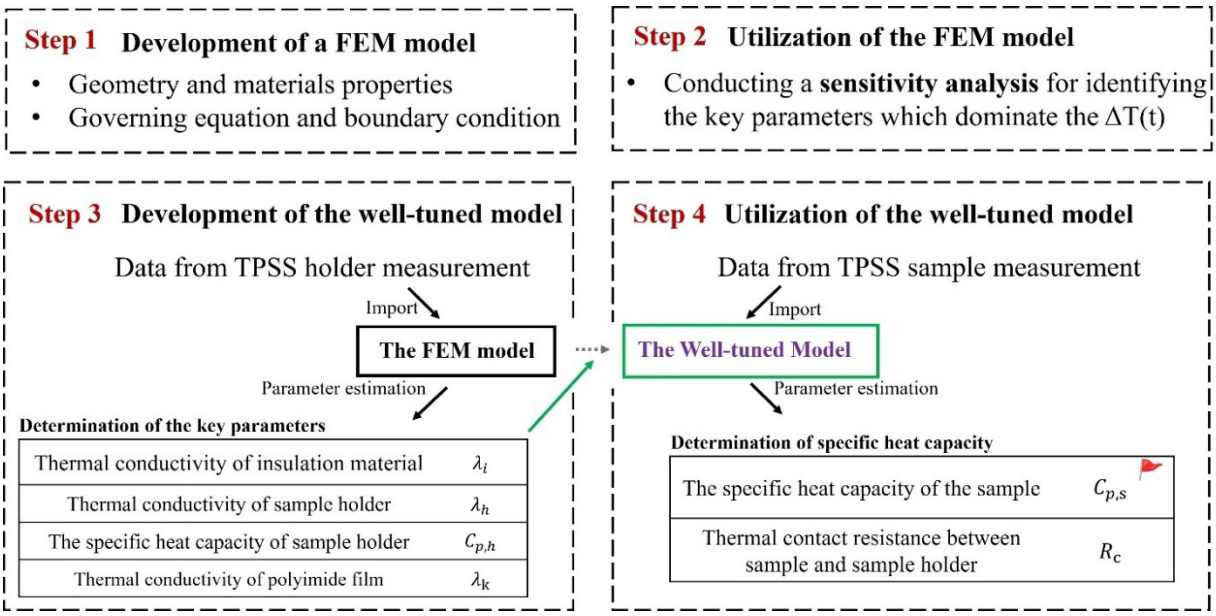

Figure 4.2. The framework for developing and utilizing the well-tuned model for the specific heat capacity determination.

4.3 Results and discussion

We initially compared the simulated $\Delta T(t)$ against the measured $\Delta T(t)$ from the holder measurement (Fig. 4.3a) and the sample measurements (Fig. 4.3b), respectively. The difference in $\Delta T(t)$ is lower than 1% in both cases, which demonstrates the reliability of the well-tuned model.

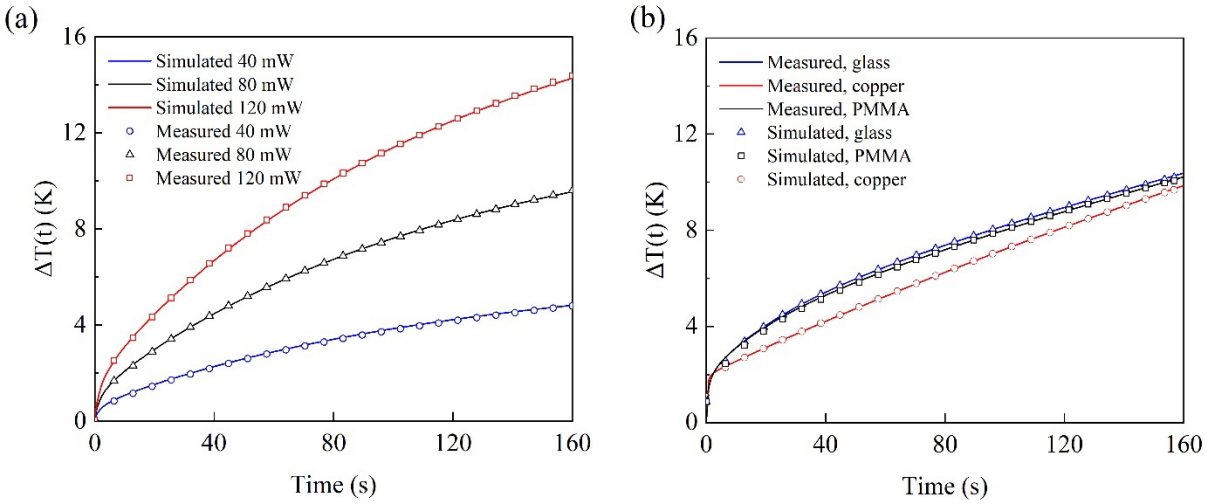

Figure 4.3. Comparison between measured $\Delta T(t)$ (symbols) and simulated $\Delta T(t)$ (solid lines) in the case of holder measurement and (b) sample measurement.

Subsequently, the specific heat capacity of the samples was extracted from the parameter estimation study based on the well-tuned model. The extracted value is in good agreement with the reference value obtained from the DSC or the Dynamic Plane Source (DPS) technique, with an average difference less than 2.4%. This demonstrates the capability of the model to determine the specific heat capacity of samples based on the measured data.

Utilizing the validated model, we analysed the heat balance during the measurement and investigated how heat loss influences the measurement accuracy.

In the holder measurement, the rate of heat accumulation into the insulation material ($Q(t)$), namely the rate of heat loss, increases over time, while the rate of heat accumulation into the sample holder shows a opposite trend (Fig. 4.4a). At the end of the measurement, the rate of heat loss significantly surpasses the later, constituting 74% of the total heating power. This suggests that heat loss predominates in the later stages of the measurement, which is undesirable.

In the sample measurement of copper, the rate of heat accumulation into the insulation material and the sample holder behaves similarly to the holder measurement (Fig. 4.4b). Although the rate of heat accumulation into the sample decreases over time, it remains the highest among the three components.

Table 4.2. Comparison between the C_p determined by the well-tuned model and the reference value. a. Measured by the DPS technique[35]. b. Measured by the DSC method.

Sample	Specific heat capacity (J/kg/K)		
	Estimated	Reference	Average difference
Copper	384 ± 8	383 ± 8^{a}	0.2 %
Glass	836 ± 17	843 ± 34^{b}	0.8 %
PMMA	1401 ± 28	1436 ± 15^{b}	2.4 %

Knowing the rate of the heat loss, we extracted and compared the heat loss equations in the holder measurement and the sample measurement, based on $f(t) = Q(t)/\frac{d}{dt}\big(\Delta T(t)\big)$.

In the measurement of copper, $f_h(t)$ closely aligns with $f_s(t)$ during 20 s to 40 s (Fig. 4.4c), consistent with the assumption $f_h(t) = f_s(t)$ in the original TPSS theory. However, the difference between $f_h(t)$ and $f_s(t)$ increases considerably over time. In the measurement of PMMA (poly(methyl methacrylate)), $f_h(t)$ is larger than $f_s(t)$ throughout the measurement, and the difference between them remains roughly constant in the later stage of the measurement.

Ultimately, we calculated the relative error in determining heat loss, referred to as the $\varepsilon_Q(t)$, using Eq. 4.1,

$$\varepsilon_Q(t) = \frac{f_r(t)\frac{d}{dt}\big(T_S(t)\big) - Q_S(t)}{P_S} \tag{4.1}$$

where Q_s is the rate of heat loss in the sample measurement. Based on the theory outlined in **Chapter 2.4**, the data from 20 s to 40 s is experimentally used in the TPSS method for calculating the C_p of copper. In the case of copper, $\varepsilon_Q(t)$ remains within ±1 % during the time interval from 20 s to 40 s (Fig. 4.4d, red region), which contributes to the accurate determination of the C_p of copper.

On the other hand, with the settling time for PMMA calculated at 120 s, the data after 120 s is experimentally utilized for the C_p of PMMA. In the stage after 120 s, however, $\varepsilon_Q(t)$ increases from 3% to 10%. This means the heat loss is overestimated, which leads to the underestimation of the specific heat capacity of the PMMA.

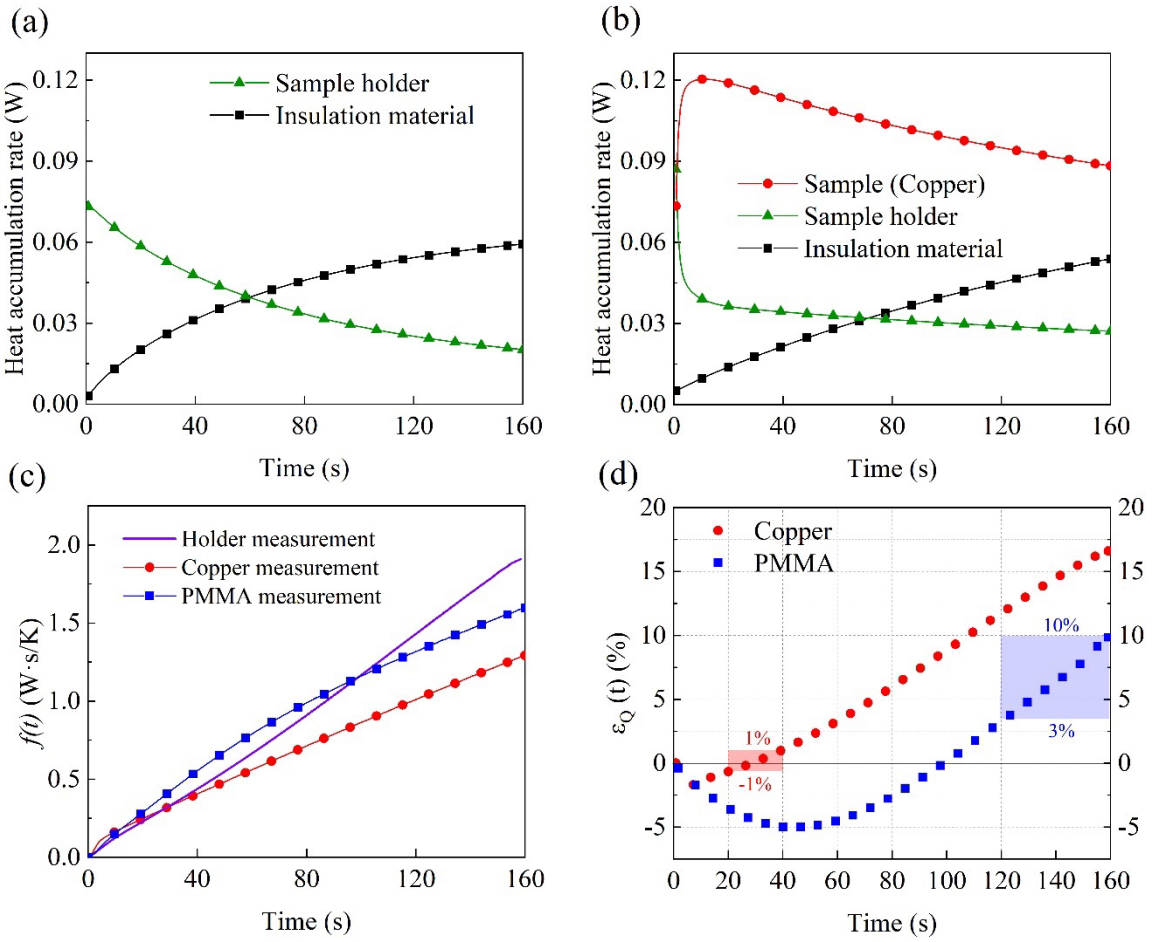

Figure 4.4. (a) The rate of heat accumulation into different components during the holder measurement and (b) the sample measurement. (c) Comparison between $f(t)$ in the holder measurement and the sample measurement of copper and PMMA. (d) The relative error of heat loss determination in the case of copper and PMMA, calculated using Eq. 4.1.

In this chapter, we developed a numerical model of the TPSS heat capacity measurement to investigates the reason for the underestimated results. The key material properties utilized in the numerical model are tuned using the holder measurement data, which enables the model to closely mimic the actual measurements. Afterwards, the model was utilized to estimate the specific heat capacity of the samples with various thermal conductivity. The estimated values proved in good agreement with the reference values. Moreover, we quantified the heat loss occurring during the holder measurement and the sample measurements. It was found that the conventional theory in TPPS method tends to overestimate the heat loss in the sample measurements, especially when measurement time is long, which results in an underestimated heat capacity.

Chapter 5

CONCLUSION AND OUTLOOK

The TPS measurement of intrinsic $\lambda_\perp$ of films

We have designed and validated a routine to extend the TPS method for measuring the intrinsic $\lambda_\perp$ of polymer films. In this routine, liquid thermal interface material is introduced for minimizing and stabilizing the thermal contact resistance. Additionally, film samples with different thickness are required for deconvoluting intrinsic $\lambda_\perp$ from the measured data, which contains the effects of thermal contact resistance. This routine is deemed reliable for film samples ranging in thickness from 80 μm to 600 μm with thermal conductivity lower than 2 W/(mK), as illustrated in Fig. 5.1.

Future work can proceed along two distinct path. The first path is the application of this refined method to investigate novel materials with unknown thermal conductivities, seeking to connect their material properties with their microstructure. The second path aims to further extend the TPS method to accommodate a broader spectrum of sample types and a larger range of measurement temperatures (T_0).

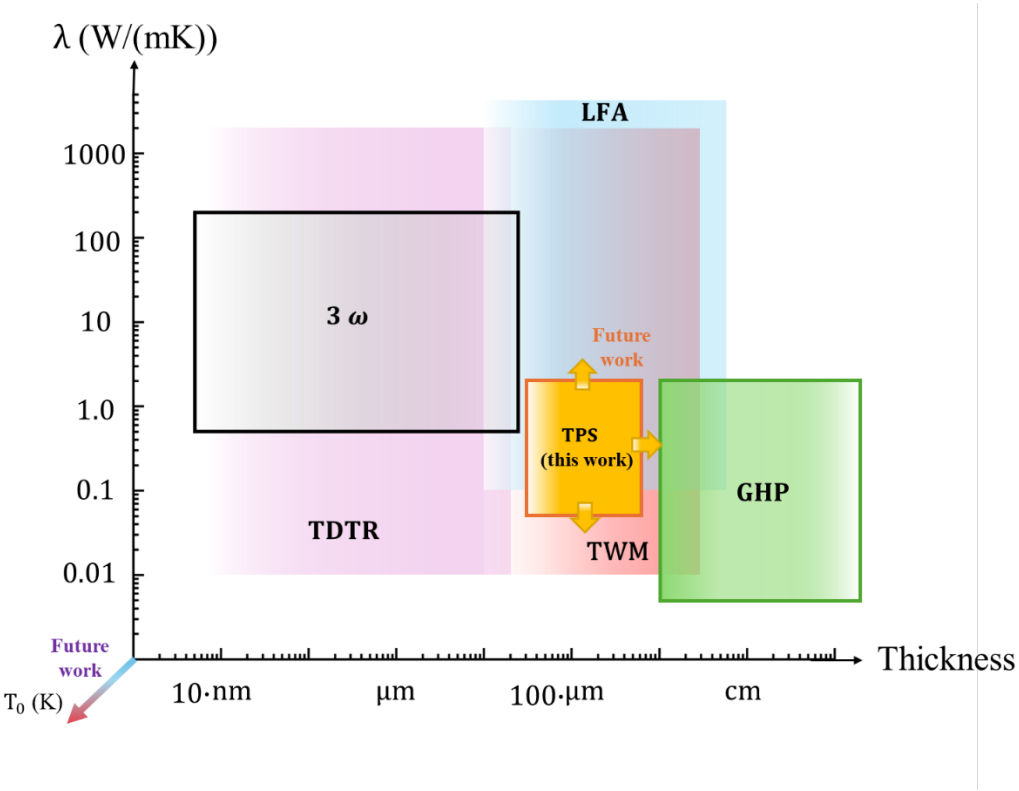

Figure 5.1. A comparison of sample size and thermal conductivity specifications across six commercial methods (TPS[29], TDTR[36], 3-ω[37], LFA[38], TWM[39] and GHP[40]). The coloured regions with frames indicates the specifications of the methods for directly measuring thermal conductivity, while the unframed areas represent those for measuring thermal diffusivity. Arrow signs denote the potential directions for future enhancement in the TPS method.

The TPSS measurement of C_p

We have developed a well-tuned numerical model that is capable of precisely mimicking the TPSS measurement of C_p. This model offers a precise estimation of heat loss during the measurement, thereby enabling the correct determination of the specific heat capacity of the samples. With the numerical model aiding data analysis, the TPSS measurement is anticipated to accurately evaluate samples with a thermal conductivity above 0.1 W/(mK)..

Future work could extend to the measurement of larger, inhomogeneous samples, such as batteries, textiles, and building composites, at temperatures reaching up to 200°C (Fig. 5.2).

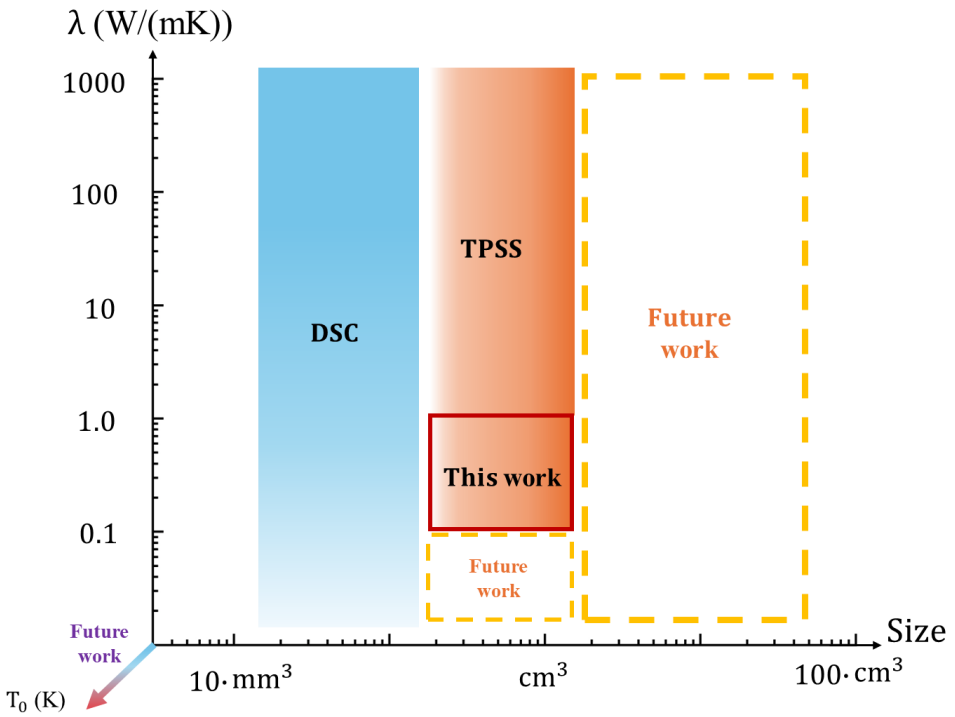

Figure 5.2. A comparison of sample size and thermal conductivity specifications between DSC[41] and the TPSS. The frames with orange dashed line indicate the potential direction of further improving the TPSS.

ACKNOWLEDGMENT

I would like to express my heartfelt gratitude to Dr. Besira Mihiretie for invaluable guidance, sharing of expertise, and kind suggestions. I extend my sincere thanks to Prof. Christian Müller for his unwavering support and ever-helpful demeanour whenever I needed assistance.

I am deeply appreciative of Dr. Silas Gustafsson for insightful discussion. My sincere thanks go to Dr. Mattias Gustavsson and Dr. Henrik Otterberg for their generous support, ensuring the smooth progress of my work at the company.

I would like to extend my appreciation to Anton, Andrey, Anders, Thomas G, Tomas N, Jesper, Johan, Albin, Teo, and Anna for being fantastic colleagues at Hot Disk!

Furthermore, I want to express my gratitude to Lotta, Mavi, Joost, Przemyslaw, Sri, Emmy, Ida, Judy, Judith, Shuichi, Youngseok, Jan, Veronica, Amin, Zewdneh, Qiannan, Monika, Krzysztof, Adil, Ulises, Josué, Pablo, Jinhui, Jinnan, Shengxi, Alexandre H, Jessica, Mathis, Lidiya, and Megan for being so nice and lovely on the 8th floor!

感谢我的父母以及所有亲人。

感谢我的爱人，感谢你一直的支持与陪伴。

BIBLIOGRAPHY

1 Zweben, C. Advances in composite materials for thermal management in electronic packaging. *Jom* **50**, 47-51 (1998).

2 Ghosh, S. *et al.* Extremely high thermal conductivity of graphene: Prospects for thermal management applications in nanoelectronic circuits. *Applied Physics Letters* **92** (2008).

3 Moore, A. L. & Shi, L. Emerging challenges and materials for thermal management of electronics. *Materials today* **17**, 163-174 (2014).

4 Xia, G., Cao, L. & Bi, G. A review on battery thermal management in electric vehicle application. *Journal of power sources* **367**, 90-105 (2017).

5 Zhang, X., Li, Z., Luo, L., Fan, Y. & Du, Z. A review on thermal management of lithium-ion batteries for electric vehicles. *Energy* **238**, 121652 (2022).

6 He, Y.-L. & Xie, T. Advances of thermal conductivity models of nanoscale silica aerogel insulation material. *Applied Thermal Engineering* **81**, 28-50 (2015).

7 Pásztory, Z. An overview of factors influencing thermal conductivity of building insulation materials. *Journal of Building Engineering* **44**, 102604 (2021).

8 Sootsman, J. R., Chung, D. Y. & Kanatzidis, M. G. New and old concepts in thermoelectric materials. *Angewandte Chemie International Edition* **48**, 8616-8639 (2009).

9 Zhang, Q., Sun, Y., Xu, W. & Zhu, D. Organic thermoelectric materials: emerging green energy materials converting heat to electricity directly and efficiently. *Advanced Materials* **26**, 6829-6851 (2014).

10 Zapata-Arteaga, O. *et al.* Reduction of the lattice thermal conductivity of polymer semiconductors by molecular doping. *ACS Energy Letters* **5**, 2972-2978 (2020).

11 ISO 8302:1991, Thermal insulation — Determination of steady-state thermal resistance and related properties — Guarded hot plate apparatus. (1991).

12 Salmon, D. Thermal conductivity of insulations using guarded hot plates, including recent developments and sources of reference materials. *Measurement Science and Technology* **12**, R89 (2001).

13 ISO 22007-4:2017, Plastics — Determination of thermal conductivity and thermal diffusivity - Part 4: Laser flash method. (2024).

14 ISO 22007-2:2022, Plastics — Determination of thermal conductivity and thermal diffusivty — Part 2: Transient plane heat source (hot disc) method.

15 Ahadi, M., Andisheh-Tadbir, M., Tam, M. & Bahrami, M. An improved transient plane source method for measuring thermal conductivity of thin films: Deconvoluting thermal contact resistance. *International Journal of Heat and Mass Transfer* **96**, 371-380 (2016).

16 Feng, B., Zhang, Y.-H., Tu, J., Fan, L.-W. & Yu, Z.-T. Determination on the thermal conductivity and thermal contact resistance of thin composite phase change films as a thermal interfacial material. *Case Studies in Thermal Engineering* **33**, 101979 (2022).

17 Gustavsson, M. & Hälldahl, L. Thermal conductivity measurements of thin insulating layers deposited on high-conducting sheets. *International journal of thermophysics* **27**, 195-208 (2006).

18 Landry, D., Flores, R. & Goodman, R. B. Estimating the Thermal Conductivity of Thin Films: A Novel Approach Using the Transient Plane Source Method. *ASME Journal of Heat and Mass Transfer* **146** (2024).

19 Dames, C. Measuring the thermal conductivity of thin films: 3 omega and related electrothermal methods. *Annual Review of Heat Transfer* **16** (2013).

20 Jiang, P., Qian, X. & Yang, R. Tutorial: Time-domain thermoreflectance (TDTR) for thermal property characterization of bulk and thin film materials. *Journal of Applied Physics* **124** (2018).
21 Cahill, D. G. Thermal-conductivity measurement by time-domain thermoreflectance. *MRS Bulletin* **43**, 782-789 (2018).
22 Schmidt, A. J. Pump-probe thermoreflectance. *Annual Review of Heat Transfer* **16** (2013).
23 Schmidt, A. J., Chen, X. & Chen, G. Pulse accumulation, radial heat conduction, and anisotropic thermal conductivity in pump-probe transient thermoreflectance. *Review of scientific instruments* **79** (2008).
24 ISO 22007-3:2008, Plastics — Determination of thermal conductivity and thermal diffusivity — Part 3: Temperature wave analysis method. (2008).
25 Hashimoto, T., Matsui, Y., Hagihara, A. & Miyamoto, A. Thermal diffusivity measurement of polymer films by the temperature wave method using joule-heating. *Thermochimica acta* **163**, 317-324 (1990).
26 Suurkuusk, J. & Wadsö, I. Design and testing of an improved precise drop calorimeter for the measurement of the heat capacity of small samples. *The Journal of Chemical Thermodynamics* **6**, 667-679 (1974).
27 ISO 19628:2017, Fine ceramics (advanced ceramics, advanced technical ceramics) Thermophysical properties of ceramic composites — Determination of specific heat capacity. (2017).
28 ISO 11357-4:2021, Plastics — Differential scanning calorimetry (DSC) — Part 4: Determination of specific heat capacity. (2021).
29 Hot Disk Thermal Constants Analyser — Instruction Manual, Hot Disk AB, Sweden. (2022).
30 Taylor, N. E., Williamson, D. M., Research, E. O. o. A. & States, D. A. U. Characterising Group Interaction Modelling for Complex Composite Materials. *European Office of Aerospace Research and Development, Arlington* (2019).
31 Gustavsson, M., Saxena, N., Karawacki, E. & Gustafsson, S. in *Thermal Conductivity 23* 56-65 (CRC Press, 2021).
32 Gustafsson, S. E. Transient plane source techniques for thermal conductivity and thermal diffusivity measurements of solid materials. *Review of Scientific Instruments* **62**, 797-804, doi:10.1063/1.1142087 (1991).
33 Berge, A., Adl-Zarrabi, B. & Hagentoft, C.-E. Determination of specific heat capacity by transient plane source. *Frontiers of Architectural Research* **2**, 476-482 (2013).
34 MatWeb, DuPont™ Kapton® 100HN Polyimide Film, 25 Micron Thickness, https://www.matweb.com/search/DataSheet.aspx?MatGUID=60f4713edc39466d89ec58f5450fdc93.
35 Karawacki, E. & Suleiman, B. M. Dynamic plane source technique for simultaneous determination of specific heat, thermal conductivity and thermal diffusivity of metallic samples. *Measurement Science and Technology* **2**, 744 (1991).
36 Thermoreflectance by Pulsed Light Heating — NanoTR/PicoTR, NETZSCH-Gerätebau GmbH, Germany.
37 Product Brochure: Thin film analyzer**,** LINSEIS GmbH, Germany.
38 Product Brochure: Light Flash Apparatus — LFA 467 HyperFlash® Series, NETZSCH-Gerätebau GmbH, Fermany.
39 Product Brochure: ai-Phase Mobile M3 type, ai-Phase Co., Ltd., Japan.
40 Guarded Hot Plate Series — GHP 500, GHP 600, GHP 900 and GHP 900 S, NETZSCH TAURUS Instruments GmbH, Germany.

41 Product Brochure: Crucibles for Thermal Analysis, METTLER TOLEDO Group, Switzerland. (2023).

Paper I

Determination of intrinsic cross-plane thermal conductivity of films through the Transient Plane Source measurements

Under review

Paper II

Extending the Transient Plane Source Scanning Method for Determining the Specific Heat Capacity of Low Thermal Conductivity Materials through a Numerical Study

Manuscript in preparation